

Hierarchical Self-Assembly of Soft Disklike Particles under Shear Flow

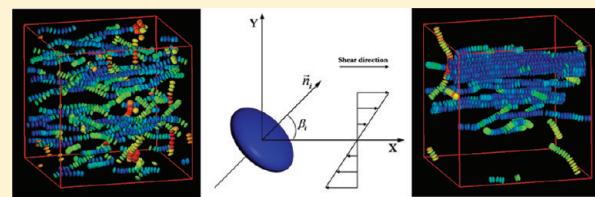
Xiao-Xi Jia,[†] Zhan-Wei Li,^{*,†} Zhao-Yan Sun,[‡] and Zhong-Yuan Lu^{*,†}

[†]Institute of Theoretical Chemistry, State Key Laboratory of Theoretical and Computational Chemistry, Jilin University, Changchun 130023, China

[‡]State Key Laboratory of Polymer Chemistry and Physics, Changchun Institute of Applied Chemistry, Chinese Academy of Sciences, Changchun 130022, China

 Supporting Information

ABSTRACT: We develop a mesoscale nonequilibrium simulation model to study the effect of steady shear on the hierarchical self-assembly of soft disklike particles in dilute solutions. By properly tuning shear rates and solvent conditions, soft disklike particles can self-assemble into flexible threads and bundle-like structures along the flow direction. Shear flow facilitates the self-assembly of soft disklike particles into one-dimensional long threads along the flow direction; however, it suppresses the formation of flexible bundles from the threads while decreasing the solvent quality. The relatively well-defined bundle structures along the flow direction can only be obtained when the solvent condition becomes even worse. Our study elucidates how the solvent condition and shear rate can be utilized to control the shear-induced self-assembled structures, which would enable designed nanofabrication.



INTRODUCTION

Hierarchical self-assembly offers a promising method to organize nanoscale objects into functional nanostructures.^{1–8} A revolution in novel anisotropic nanoparticles and colloidal building blocks has brought new excitement to this field.⁹ Self-assembly of these nonmolecular building blocks is mainly based on selective control of noncovalent interactions.¹⁰ At present, various novel structures can be fabricated by the self-assembly of exotic building blocks including patchy particles,^{11–13} Janus particles,^{14,15} polyhedral metal plates,¹⁶ disklike ellipsoidal particles,¹⁷ and so on.

Soft anisotropic particles, such as soft patchy particles,¹⁸ soft disklike micelles,^{6,19} and soft disklike molecules,²⁰ may be also used as important building blocks for further hierarchical self-assembly due to their anisotropic interactions and shapes. Wooley and co-workers reported that the anisotropic shape of disklike micelles allows for one-dimensionally preferred growth in experiments.⁶ Palazzo and co-workers suggested that a nematic columnar phase can originate in a system of negatively charged disk-shaped micelles, probably stabilized by weak attractions.²¹ We had studied ordered packing of a soft discoidal system with the aid of the mesoscale simulation model and obtained a relatively ordered hexagonal column structure.²² We had also proposed a mesoscopic model to investigate the hierarchical self-assembly of soft disklike particles in dilute solutions²³ and found that the cooperative driving factors for the self-assembly are the weak noncovalent attraction and phase separation: the weak attraction allows soft disklike particles to self-assemble into one-dimensional threads and the phase separation does not break the one-dimensional thread structures

but brings the threads together to form a hexagonal bundle structure.

Actually, in experiments and during processing, the nonequilibrium conditions are commonly encountered. Shear-induced clustering, ordered packing, orientational alignment, and structural changes in soft matter systems are of considerable interest both from fundamental and application viewpoint.^{24–28} Many soft matter systems, ranging from block copolymers^{29–33} to wormlike micelles,^{34–36} rodlike micelles,³⁷ vesicles,²⁴ colloidal particles,^{38–40} liquid crystals,^{41–43} nanorods,^{44,45} and nanotubes,^{46,47} have been investigated under shear-flow conditions. Among these nonequilibrium systems, a majority of studies have involved anisotropic particles because shear can influence both the texture and the orientation of the anisotropic species.²⁷ Anisotropic particles are also of major practical relevance since the orientation of the particles in a fluid will substantially affect the physical and optical properties of the final products.⁴⁸ Thus, it is very important to investigate the self-assembly of soft disklike particles under shear flow in order to design new hierarchical structures.

In this study, we develop a mesoscale nonequilibrium simulation model that can reflect the interaction nature between soft disklike particles and their shear-alignment behavior in a simple way and thus allows one to study hierarchical self-assembly of soft disklike particles under steady shear. With this nonequilibrium model, we investigate the effect of steady shear on the self-assembled structures and the orientations of soft disklike

Received: June 17, 2011

Revised: October 6, 2011

Published: October 10, 2011

particles in dilute solutions and mainly focus on the influences of shear rate and solvent condition on the self-assembled thread and bundle structures.²³

■ MODEL AND SIMULATION DETAILS

In the following, we use the interaction cutoff radius as the unit of length, $r_c = 1$, $k_B T$ as the unit of energy, $k_B T = 1$, and choose the moment of inertia and the mass of the particle as the units, i.e., $I = m = 1$ for simplicity; thus, the time unit $\tau = (mr_c^2/k_B T)^{1/2} = 1$. On the basis of the soft conservative potential in dissipative particle dynamics (DPD),^{49,50} we proposed in a recent paper²³ an anisotropic potential to reflect the interaction nature between soft disklike particles (i.e., a mesoscale particle dynamics method). It is expressed as

$$U_{ij} = \frac{\alpha_{ij}^R}{2} (1 - r_{ij})^2 - f^\nu \frac{\alpha_{ij}^A}{2} (r_{ij} - r_{ij}^2) \quad (1)$$

where

$$f = \frac{(\mathbf{n}_i \cdot \mathbf{r}_{ij})(\mathbf{n}_j \cdot \mathbf{r}_{ij})}{r_{ij}^2} \quad (2)$$

and \mathbf{n}_i and \mathbf{n}_j are unit vectors assigning the orientation to particle i and j , respectively.⁴⁹ The anisotropic factor f is unity if both \mathbf{n}_i and \mathbf{n}_j are parallel to \mathbf{r}_{ij} (the vector connecting the particles i and j). If either \mathbf{n}_i or \mathbf{n}_j or both is perpendicular to \mathbf{r}_{ij} then $f = 0$. If either \mathbf{n}_i or \mathbf{n}_j is antiparallel to \mathbf{r}_{ij} , then $f^\nu = -1$ for ν odd, and $f^\nu = 1$ for ν even. If we define that θ_i is the angle between \mathbf{n}_i and \mathbf{r}_{ij} , and θ_j is the angle between \mathbf{n}_j and \mathbf{r}_{ij} then eq 1 can be rewritten as

$$U_{ij} = \frac{\alpha_{ij}^R}{2} (1 - r_{ij})^2 - (\cos \theta_i \cos \theta_j)^\nu \frac{\alpha_{ij}^A}{2} (r_{ij} - r_{ij}^2) \quad (3)$$

Here, the magnitude of α_{ij}^R controls the strength of repulsion, α_{ij}^A controls the strength of attraction, and ν controls the angular width of the attraction. Thus, both α_{ij}^A and ν will control the flexibility of the particle aggregates.

In eq 3, when $\theta_i = \theta_j = 0^\circ$, explicitly weak attraction between particles will arise at long-range of the anisotropic potential. This is phenomenologically designed to reflect the weak hydrogen bonding or hydrophobic interactions between two approaching disklike particle surfaces. The strength of the attraction will decrease with increasing θ_i . If θ_i reaches 90° , then $f = 0$ and eq 3 becomes the standard DPD repulsive potential $U_{ij} = (\alpha_{ij}/2)(1 - r_{ij})^2$. For the attractive potential $U_{ij} = (\alpha_{ij}^R/2)(1 - r_{ij})^2 - (\alpha_{ij}^A/2)(r_{ij} - r_{ij}^2)$, we presented a parabola fitting between the calculated average pressure and the number density and suggested that the simulation model can still be described well by the Flory–Huggins-type equation of state, which implies that the intrinsic length scale of the proposed potential is on mesoscale.²³

The anisotropic force between two disklike particles is then given by the derivation of eq 1

$$\begin{aligned} \mathbf{F}_{ij} = & \alpha_{ij}^R (1 - r_{ij}) \frac{\mathbf{r}_{ij}}{r_{ij}} + \alpha_{ij}^A f^\nu \left(\frac{1}{2} - r_{ij} \right) \frac{\mathbf{r}_{ij}}{r_{ij}} \\ & + \frac{\alpha_{ij}^A}{2r_{ij}} (r_{ij} - r_{ij}^2) \nu f^{\nu-1} \left[\frac{(\mathbf{n}_i \cdot \mathbf{r}_{ij}) \mathbf{n}_j}{r_{ij}} + \frac{(\mathbf{n}_j \cdot \mathbf{r}_{ij}) \mathbf{n}_i}{r_{ij}} - 2f \frac{\mathbf{r}_{ij}}{r_{ij}} \right] \end{aligned} \quad (4)$$

The translational displacements of disklike particles follow the Newton's equations of motion. The equations of rotational

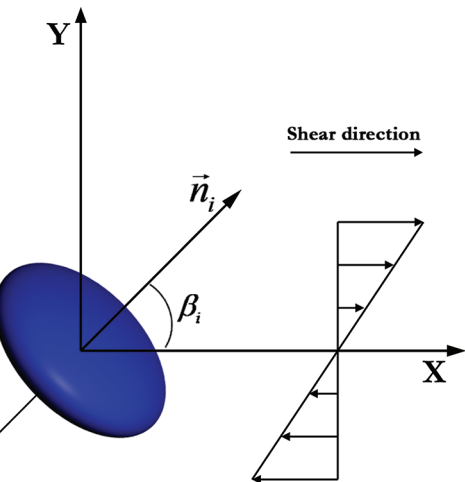


Figure 1. Coordinate system for disklike particle i centered at the origin and subjected to a simple shear in XY plane. The flow direction is parallel to the X axis, the velocity gradient is along the Y axis. For the sake of clarity, the Z axis is not shown, which represents the vortex direction. \mathbf{n}_i is the unit vector assigning the orientation to disklike particle i , and β_i is the angle between the direction vector \mathbf{n}_i of disklike particle i and the direction of shear (X axis).

motion can be written as⁵¹

$$\dot{\mathbf{n}}_i = \mathbf{u}_i \quad (5)$$

$$\dot{\mathbf{u}}_i = \mathbf{g}_i^\perp / I + \lambda \mathbf{n}_i \quad (6)$$

where I is the moment of inertia. Equation 5 simply defines \mathbf{u}_i as the time derivative of the orientation \mathbf{n}_i . Physically, the first term in eq 6 corresponds to the perpendicular component of \mathbf{g}_i responsible for rotation of the particle, where

$$\mathbf{g}_i^\perp = \mathbf{g}_i - (\mathbf{g}_i \cdot \mathbf{n}_i) \mathbf{n}_i \quad (7)$$

with

$$\mathbf{g}_i = \frac{\alpha_{ij}^A}{2} (r_{ij} - r_{ij}^2) \nu f^{\nu-1} \frac{(\mathbf{n}_j \cdot \mathbf{r}_{ij}) \mathbf{r}_{ij}}{r_{ij}^2} \quad (8)$$

The second term in eq 6 corresponds to the force $\lambda \mathbf{n}_i$ along the vector \mathbf{n}_i which constrains the vector length to be a constant of the motion.⁵¹ The equations of both translational and rotational motions are integrated via a half-step leapfrog algorithm.^{51,52} In the rotational motion, a full step in the integration algorithm is advanced through the equation

$$\begin{aligned} \mathbf{u}_i \left(t + \frac{1}{2} \delta t \right) = & \mathbf{u}_i \left(t - \frac{1}{2} \delta t \right) \\ & + \delta t \mathbf{g}_i^\perp(t) / I - 2 \left[\mathbf{u}_i \left(t - \frac{1}{2} \delta t \right) \cdot \mathbf{n}_i(t) \right] \mathbf{n}_i(t) \end{aligned} \quad (9)$$

The step is completed using

$$\mathbf{n}_i(t + \delta t) = \mathbf{n}_i(t) + \delta t \mathbf{u}_i \left(t + \frac{1}{2} \delta t \right) \quad (10)$$

To impose steady shear, the Lees–Edwards periodic boundary conditions^{51,53} are employed to set up and maintain a steady linear velocity profile with gradient $\dot{v} = \partial v_X / \partial x_X$. As shown in Figure 1, the flow direction is parallel to the X axis, the velocity gradient is along the Y axis, and the Z axis represents the vortex

direction. The applied velocity gradient induces velocity and angular velocity fields \mathbf{V} and $\boldsymbol{\Omega}$, respectively, which must be taken into account in defining specific disklike particle velocities

$$\mathbf{v}'_i = \mathbf{v}_i - \mathbf{V} \quad (11)$$

$$\mathbf{u}'_i = \mathbf{u}_i - \boldsymbol{\Omega} \quad (12)$$

where \mathbf{v}_i is the velocity and \mathbf{u}_i the angular velocity of particle i .^{54,55} Here, we assume that the velocity gradient $\dot{\gamma}$ is constant everywhere, and \mathbf{V} and $\boldsymbol{\Omega}$ are time independent (i.e., no turbulence is induced). The shear flow profile is given by

$$\mathbf{V} = \dot{\gamma} r \mathbf{i}_X \quad (13)$$

Furthermore, we assume that $\boldsymbol{\Omega}$ is independent of position, depending only on the orientation of disklike particle.⁵⁴ $\boldsymbol{\Omega}$ is given by

$$\boldsymbol{\Omega} = \dot{\gamma} \cos^2(\beta_i) \quad (14)$$

where β_i is the angle between the direction vector \mathbf{n}_i of particle i and the direction vector \mathbf{E}_X of shear flow. Equation 14 means that the shear flow tends to align a disklike particle with direction vector \mathbf{n}_i perpendicular to the flow direction \mathbf{E}_X .^{54,56}

The simulations are performed in canonical ensemble. The weak coupling Berendsen thermostat,⁵² instead of other temperature control schemes in DPD,⁵⁷ is used to control of temperature at the target value. We simulate systems of 2.4×10^4 particles in a $20 \times 20 \times 20$ cubic box with periodic boundary conditions. The number of disklike solute particles is $N_{\text{solute}} = 24000 \times \phi$, and the number of spherical solvent particles is $N_{\text{solvent}} = 24000 \times (1 - \phi)$ (ϕ is the concentration of the disklike solute particles). The solute–solvent and solvent–solvent interactions follow the first term of eq 1. A time step $\delta t = 0.001$ is used.

RESULTS AND DISCUSSION

In general, the second virial coefficient ν_2 can provide a quantitative measure of the tendency of a fluid to phase separate (i.e., aggregate or precipitate).⁴⁵ For a dilute suspension of hard rods, ν_2 can be written as^{45,58–60}

$$\nu_2 = 2L^2D[1 - (0.035 + \varepsilon_{\text{att}})S_2^2 - O(\varepsilon_{\text{att}}D/L)] \quad (15)$$

Actually, ν_2 can also be used to give a better understanding of the aggregation phenomena of soft disklike particles, since their anisotropic shape is quite similar to that of hard rods. Here, ε_{att} denotes the strength of attraction between soft disklike particles, $S_2 = \langle P_2(\cos \theta) \rangle$ with P_2 denoting the Legendre polynomial and θ the angle between soft disklike particle direction vector and the axis of alignment, represents the orientational order parameter of soft disklike particles,⁴⁵ and L and D are the thickness and the diameter of the disklike particles, respectively. From eq 15, it is clear that we may enforce soft disklike particles to aggregate by enhancing the strength of attraction (ε_{att}) and/or by increasing the orientational order parameter (S_2). Thus in our simulations, we change shear flow to modulate S_2 and try to elucidate the effect of shear flow on the self-assembly of soft disklike particles in dilute solution.

In the simulations, increasing the repulsion strength α_{12}^R between the disklike solute particle and the solvent particle in eq 1 corresponds to varying the solvent condition, which may be induced by cooling or adding another nonsolvent in experiments. Therefore, in order to investigate the effect of steady shear on the

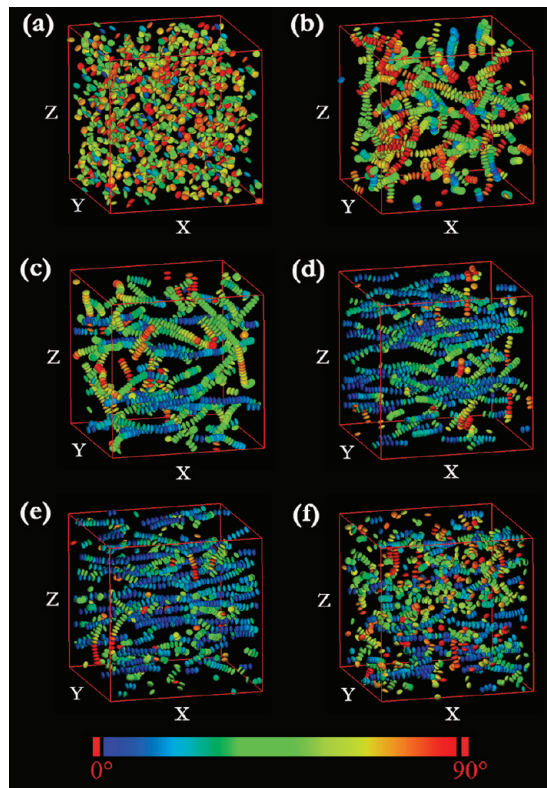


Figure 2. Typical packing structures of the systems with $\alpha_{12}^R = 250$ at different shear rates $\dot{\gamma}$: (a) initial configuration, (b) $\dot{\gamma} = 0.001$, (c) 0.01, (d) 0.1, (e) 0.3, and (f) 0.5. The color code indicates the orientation according to the palette, and each particle i is colored depending on the absolute value of the angle between the direction vector \mathbf{n}_i of particle i and the director \mathbf{n} for orientation order (from 0° to 90°). For the sake of clarity, we only show the disklike solute particles in these systems.

self-assembly of disklike particles in dilute solution, we choose $\alpha_{11}^R = \alpha_{22}^R = 250$ (1: solute particle; 2: solvent particle), $\nu = 6$, $\alpha_{11}^A = 120$, and $\phi = 5\%$ as in ref 23 and mainly examine the influences of the shear rate $\dot{\gamma}$ and the solvent condition α_{12}^R on the self-assembled structures.

Actually, in DPD, the repulsion parameter is related to the Flory–Huggins χ parameter⁵⁰ via $\alpha_{ij} = \alpha_{ii} + 3.27\chi_{ij}$. Thus, the solvent condition α_{12}^R may be also related to the Flory–Huggins parameter χ_{12} by

$$\chi_{12} = 0.306(\alpha_{12}^R - \alpha_{11}^R) \quad (16)$$

If our model is applied to describe soft disklike micelles in ref 6, the thickness of the disklike particle L in our simulations will be roughly 25 nm, as that indicated in ref 6. We had shown in ref 23 that $L \approx 0.45r_c$ and the aspect ratio (L/D) of the disklike particle $L/D = 0.50$. Thus, the diameter of the disklike particle D is about 50 nm, and the reduced unit of length r_c approximately corresponds to $r_c^{\text{SI}} = 55$ nm in SI Units. If we assume that the density of the disklike micelle is 1.0 g/cm^3 , then the mass of the representative disklike particle will be about $m^{\text{SI}} = 4.91 \times 10^{-20} \text{ kg}$. Accordingly, the time unit $\tau = (mr_c^2/k_B T)^{1/2}$ approximately corresponds to $\tau^{\text{SI}} = 1.9 \times 10^{-7} \text{ s}$. As mentioned above, $\dot{\gamma} = \partial v_X / \partial v_X$ and the time step $\delta t = 0.001$, thus, the unit of shear rate defined in a time step δt , $\dot{\gamma}^{\text{SI}} = (r_c^{\text{SI}}/\tau^{\text{SI}}\delta t)/10r_c^{\text{SI}} \approx 526 \text{ s}^{-1}$ (i.e., $\dot{\gamma} = 1$ in the simulations corresponds to the shear rate 526 s^{-1} in real experiments).

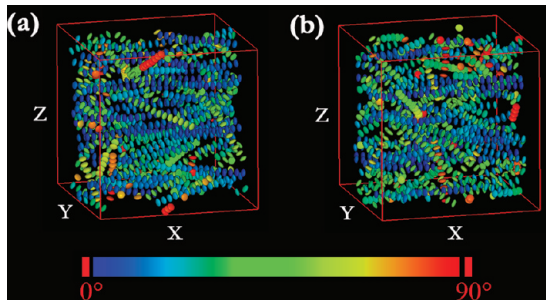


Figure 3. Self-assembled one-dimensional threads along the flow direction with $\dot{\gamma} = 0.5$ for different solvent conditions: (a) $\alpha_{12}^R = 10$ and (b) 20.

Effect of Steady Shear on the Self-Assembled Thread Structures. First of all, we keep soft disklike particles in athermal solvent condition with $\alpha_{12}^R = 250$ ($\chi_{12} \approx 0$), and examine the influence of the shear rate $\dot{\gamma}$ on the self-assembled thread structures. In order to observe the effects of the weak, moderate, and strong shear flows on the self-assembly of soft disklike particles, we set the selected shear rates $\dot{\gamma}$ to 0.001, 0.01, 0.1, 0.3, and 0.5 in reduced units (i.e., 0.52, 5.26, 52.6, 157.8, and 263 s⁻¹ in SI units), respectively. We check the achievement of the steady state in our simulations mainly by the snapshots of the systems at different time steps and the time evolution of the order parameters (introduced in the following section). If the structures of the systems at different time steps are very similar and the order parameters reach the stable values, the systems achieve the steady states. Moreover, we have also simulated the systems from different initial configurations to check the steady states.

Figure 2 shows typical packing structures under different shear rates. These snapshots are generated by Qt-based molecular graphics application (QMGA).⁶¹ Each of the nonequilibrium simulations starts from the same initially isotropic configuration as shown in Figure 2a. At the weak shear rate $\dot{\gamma} = 0.001$, the disklike particles can self-assemble into one-dimensional short threads without specific orientation as that reported in ref 23 (Figure 2b), thus the weak shear flow has no noticeable effect on the self-assembled thread structures. With increasing shear rate ($\dot{\gamma} = 0.01$), the disklike particles can self-assemble into relatively longer threads, and parts of these threads take the orientation parallel to the flow direction (Figure 2c). When moderate shear rates ($\dot{\gamma} = 0.1$ and 0.3) are applied, relatively longer threads along the flow direction can be observed, as shown in Figure 2, panels d and e. Keeping on increasing the shear rate ($\dot{\gamma} = 0.5$), the threads will be broken by the shear flow, and separated disklike particles are observed, as shown in Figure 2f. In equilibrium, the disklike particles can self-assemble into one-dimensional threads in slightly good to slightly bad solvent conditions (i.e., in parameter range $200 \leq \alpha_{12}^R \leq 270$).²³ But under shear flow, we find that, even in very good solvent conditions (for example, $\alpha_{12}^R = 10$ and 20), the disklike particles can still self-assemble into one-dimensional threads along the flow direction, as shown in Figure 3. When the shear is stopped, the self-assembled thread structures will decompose into disklike particles again. Thus this ordered structure formation due to external field is very similar to dynamic self-assembly.⁶²

In order to describe the influence of the shear rate $\dot{\gamma}$ on the self-assembled structures of soft disklike particles quantitatively,

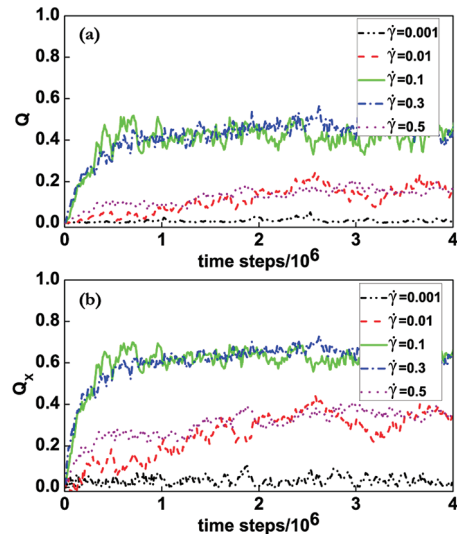


Figure 4. Time evolution of (a) the orientation order parameter (Q), and (b) the orientation order parameter along the flow direction (Q_x) for different shear rates while keeping $\alpha_{12}^R = 250$.

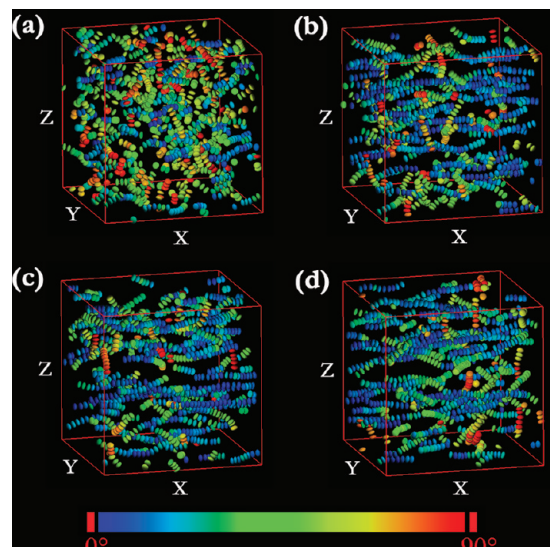


Figure 5. Snapshots of the system with $\alpha_{12}^R = 250$ and $\dot{\gamma} = 0.1$, after (a) 1×10^5 , (b) 5×10^5 , (c) 1×10^6 , and (d) 4×10^6 time steps of simulation.

we calculate the orientation order parameter Q ^{22,23,63,64} defined by

$$Q = \frac{2}{(N-1)N} \left\langle \sum_i \sum_{j>i} \frac{1}{2}(3\cos^2 \theta_{ij} - 1) \right\rangle \quad (17)$$

Here θ_{ij} is the angle between \mathbf{n}_i and \mathbf{n}_j . Note that $\theta_{ij} = 0$ corresponds to $Q = 1$, whereas random orientations of \mathbf{n}_i result in $Q = 0$. We have also calculated the orientation order parameter parallel to the flow direction, Q_x , which gives information about the arrangement of disklike particles along the flow direction

$$Q_x = \frac{2}{(N-1)N} \left\langle \sum_i \sum_{j>i} \frac{1}{2}(3\cos^2 \beta_i - 1) \right\rangle \quad (18)$$

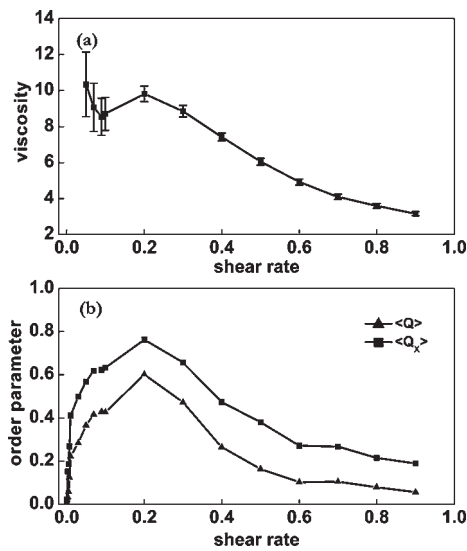


Figure 6. (a) Calculated shear viscosity and (b) the average orientation order parameters $\langle Q \rangle$ and $\langle Q_x \rangle$ with $\alpha_{12}^R = 250$ at different shear rates.

Q_X takes unity when all disklike particles align along the flow direction (X axis) and zero when disklike particles take random orientations.

Figure 4 shows the time evolution of Q and Q_X from an initially isotropic configuration for different shear rates. As shown in Figure 4a and b, under the weak shear with $\dot{\gamma} = 0.001$, $Q \approx 0$, and $Q_X \approx 0$, which indicate that the one-dimensional short threads (as shown in Figure 2b) take random orientations. With increasing shear rate, both Q and Q_X become larger. When $\dot{\gamma} = 0.1$ and 0.3 , Q and Q_X can quickly reach to the steady values with $Q \approx 0.4$ and $Q_X \approx 0.6$ after only about 1×10^6 time steps, which are clear evidence for the emergence of shear-induced long thread structures along the flow direction. Therefore, the effect of shear flow on soft disklike particles is very similar to shear-induced alignment of rods in the flow direction.⁴⁵ Further increasing the shear rate, the strong shear flow will eventually break the thread structures, both Q and Q_X fall into relatively small values again, as shown in Figure 4, panels a and b.

Typical snapshots during the evolution of the longer threads along the flow direction starting from an initially isotropic phase, are shown in Figure 5. The disklike particles first self-assemble into short threads in a short time, as shown in Figure 5a. Then, the shear flow induces a common orientation of the short threads along the flow direction, leads to interthread connections (Figure 5b), and results in a transition from short threads to relatively longer threads (Figure 5, panels c and d). As shown in Figure 5c, after 1×10^6 time steps, the relatively longer threads along the flow direction can be observed. The transition from short threads to relatively longer threads is very similar to the structure evolution of CTAB/NapTS micelles reported in ref 37. Thus, the relatively longer threads along the flow direction may be attributed to shear-thickening at moderate shear rates.

Rheological measurements can be performed to help the understanding of different shear-induced behaviors.^{30,37,65} The calculated shear viscosity,³⁰ and the average orientation order parameters $\langle Q \rangle$ and $\langle Q_X \rangle$ under different shear rates are shown in Figure 6. It is shown that the dependence of shear viscosity on shear rate can be roughly divided into three regions, which relate to different packing structures shown in Figure 2. The first region

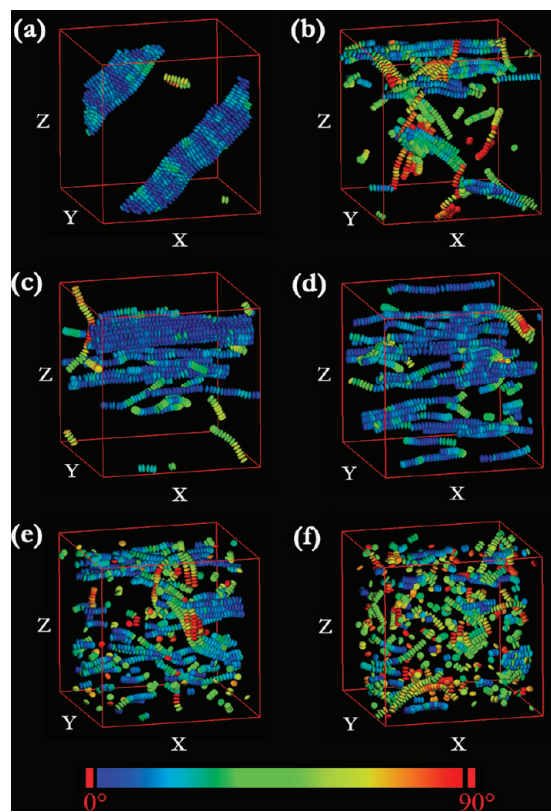


Figure 7. Typical packing structures of the systems with $\alpha_{12}^R = 330$ at different shear rates: (a) $\dot{\gamma} = 0.001$, (b) 0.05 , (c) 0.1 , (d) 0.3 , (e) 0.5 , and (f) 0.7 .

corresponds to the weak shear rates with $\dot{\gamma} < 0.09$, where the shear viscosity decreases dramatically and the average orientation order parameters $\langle Q \rangle$ and $\langle Q_X \rangle$ rapidly increase with increasing shear rate, in harmony with the phenomenon that parts of the threads taking the orientation parallel to the flow direction as shown in Figure 2c. Then, the shear viscosity first increases and decreases again from $\dot{\gamma} = 0.09$ to 0.3 and shows a local maximum at $\dot{\gamma} = 0.2$, and the average orientation order parameters $\langle Q \rangle$ and $\langle Q_X \rangle$ also reach the maximum values. In this region, the disklike particles can self-assemble into relatively longer threads along the flow direction, as shown in Figure 2d and e. After that, Both the shear viscosity and the average orientation order parameters $\langle Q \rangle$ and $\langle Q_X \rangle$ decrease gradually with increasing shear rate in the third region from $\dot{\gamma} = 0.4$ to 0.9 , where the threads will be broken by the shear flow, and separated disklike particles are observed, as shown in Figure 2f. In general, the shear viscosity decreasing with increasing shear rate corresponds to the shear-thinning, whereas the local maximum of the shear viscosity at $\dot{\gamma} = 0.2$ corresponds to the shear-thickening. Therefore, the obtained relatively longer threads along the flow direction at moderate shear rates are actually in accordance to shear-thickening. In this research, the moderate shear (from $\dot{\gamma} = 0.09$ to 0.3) will enhance the self-assembly of disklike particles into longer threads along the flow direction.

As shown above, the weak shear has no noticeable effect on the self-assembled thread structures. At moderate shear rates, the disklike particles can self-assemble into relatively longer threads along the flow direction. The strong shear will break the threads into disklike particles again. In fact, for a single disklike particle,

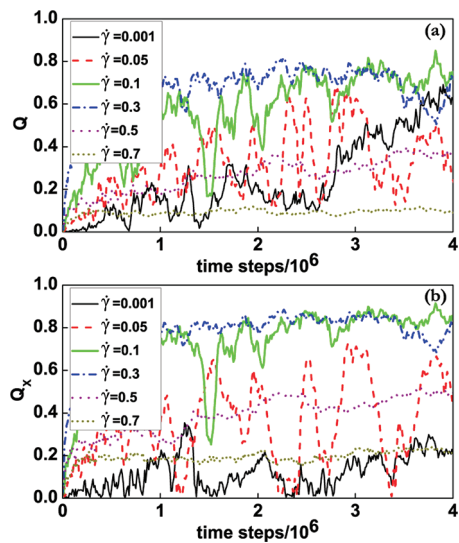


Figure 8. Time evolution of (a) the orientation order parameter (Q) and (b) the orientation order parameter along the flow direction (Q_x) for different shear rates while keeping $\alpha_{12}^R = 330$.

shear flow tends to align it with its direction vector perpendicular to the flow direction. However, the weak attraction allows the disklike particles to self-assemble into short threads, and then the shear flow tends to align the short threads along the flow direction, further leads to interthread connection, and finally results in a relatively longer threads with the particle direction vector parallel to the flow direction. This is why the orientation of disklike particles is frustrated from perpendicular to parallel to the flow direction while self-assemble into ordered structures.

Effect of Steady Shear on the Self-Assembled Bundle Structures. As reported in ref 23, in equilibrium, when the solvent condition becomes bad (i.e., the repulsion strength α_{12}^R is equal to, or larger than the critical repulsion parameter for phase separation, which is about $\alpha_{12}^R = 270$ for the concentration of the disklike particles $\phi = 5\%$), phase separation will take place. Eventually the threads approach to each other, and the disklike particles can self-assemble into hexagonal bundle structures. Thus following ref 23, we also choose $\alpha_{12}^R = 330$ ($\chi_{12} = 24.48$) and examine the influence of the shear rate $\dot{\gamma}$ on the self-assembled bundle structures.

Figure 7 shows typical packing structures at different shear rates. Each of the simulations starts from the same initially isotropic configuration as shown in Figure 2a. At weak shear rate $\dot{\gamma} = 0.001$, the disklike particles can self-assemble into flexible bundle structure as reported in ref.²³ But, as shown in Figure 7a, the bundle structure is not oriented to a certain direction such as parallel or perpendicular to the flow direction. Thus, the weak shear also has no noticeable effect on the self-assembled bundle structures. With increasing shear rate, for example $\dot{\gamma} = 0.05$, we observe the intermediate phase characterized by the coexistence of threads and bundle-like structures as shown in Figure 7b, which are partly oriented to the direction parallel to the flow direction. When moderate shear rate ($\dot{\gamma} = 0.1$) is applied, the bundle-like structures along the flow direction can be observed, as shown in Figure 7c. However, it seems that further phase separation may be needed to obtain relatively well-defined bundle structures along the flow direction. Keeping on increasing the shear rates ($\dot{\gamma} = 0.3$), shear flow suppresses the phase

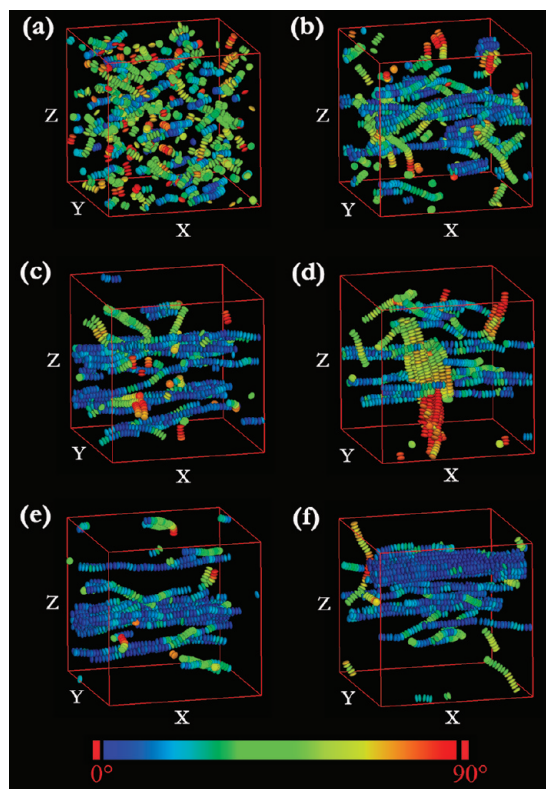


Figure 9. Snapshots of the system with $\alpha_{12}^R = 330$ and $\dot{\gamma} = 0.1$, after (a) 1×10^5 , (b) 5×10^5 , (c) 1×10^6 , (d) 1.5×10^6 , (e) 3×10^6 , and (f) 4×10^6 time steps of simulation.

separation of the threads into flexible bundles, and we observe the thread-like structures along the flow direction, as shown in Figure 7d. Further increasing $\dot{\gamma}$, the strong shear flow will break the bundle-like structures into short bundles, threads and separated disklike particles, as can be seen in Figure 7, panels e and f. To assess the system size effect, larger boxes with $32 \times 32 \times 32$ (98 304 particles) are simulated for selected state points. We also observe the self-assembled structures such as threads and bundle-like structures for larger systems, as shown in Supporting Information, Figure S1. So the finite size effect is negligible in our simulations. In the simulations, we study the systems of soft disklike particles in a cubic box with periodic boundary conditions, thus the shear directions along X , Y , and Z axes should be equivalent. To observe the influence of different shear directions, we also perform simulations with shear along Y and Z axes, respectively. We can also obtain the threads and bundle-like structures along the flow directions, as shown in Supporting Information, Figure S2. Therefore, the choice of the shear direction has no influence on the shear-induced self-assembled structures.

To analyze the influence of $\dot{\gamma}$, we also show the time evolution of Q and Q_x for different shear rates in Figure 8, panels a and b. At $\dot{\gamma} = 0.001$, the orientation order parameter Q reaches to a relatively large value about 0.5 after 3×10^6 time steps, but Q_x remains a very small value. The values of Q and Q_x validate the presence of the bundle structures without a fixed alignment orientation. With increasing shear rate, Q and Q_x become larger. The fluctuations at $\dot{\gamma} = 0.05$ may be attributed to the rotation of short thread and bundle-like structures. When $\dot{\gamma} = 0.1$, Q is about 0.7, and Q_x is about 0.8. The larger values of both Q and Q_x

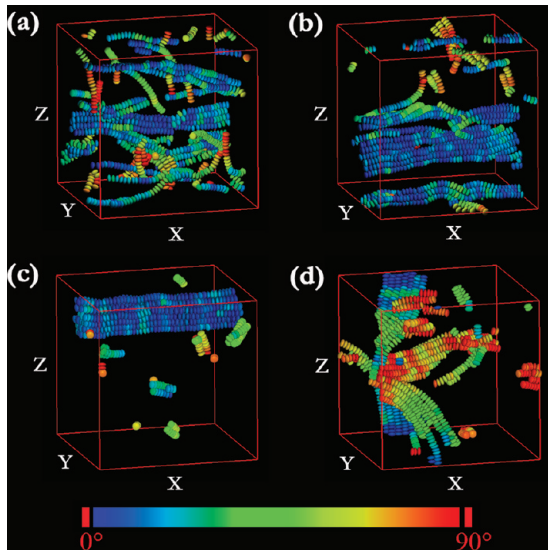


Figure 10. Typical packing structures of the systems with $\dot{\gamma} = 0.1$ for different α_{12}^R : (a) $\alpha_{12}^R = 300$, (b) 370, (c) 400, and (d) 450.

indicate that the ordered packing of disklike particles is along the flow direction, while the corresponding bundle-like structures, as shown in Figure 7c, are indeed along the flow direction. The thread structures at the shear rate $\dot{\gamma} = 0.3$ in Figure 7d are also oriented along the flow direction. At strong shear rates, both Q and Q_X become relatively small, which correspond to the disappearance of orientational order.

In order to monitor the formation process of the bundle-like structures as shown in Figure 7c, typical snapshots during the evolution of the bundle-like structures starting from an initially isotropic phase are shown in Figure 9. As shown in Figure 9a, the disklike particles also first self-assemble into short threads in the beginning of self-assembly, very similar to the case as demonstrated in Figure 5a. Then, shear flow will align the short threads along the flow direction, leads to connections between short threads, and results in a transition from short threads to relatively longer bundle-like structures (Figure 9, panels b and c). As shown in Figure 9d, shear flow can also induce the rotation of the relatively longer bundle-like structures, and leads to further connections between these bundle-like structures. It should be noted that the shear-induced rotation of the short threads and bundle-like structures may cause the fluctuations in the time evolution of Q and Q_X as shown in Figure 8. Finally, after 3×10^6 time steps, the long bundle-like structures with some defects along the flow direction can be obtained, as shown in Figure 9, panels e and f. If we want to obtain relatively well-defined bundle structures along the flow direction, further phase separation may be needed.

Increasing the repulsion strength α_{12}^R corresponds to varying the solvent condition. Thus, in order to obtain the relatively well-defined bundle structures along the flow direction, we also examine the influence of α_{12}^R on the self-assembled bundle structures while keeping $\dot{\gamma} = 0.1$. Figure 10 shows typical packing structures in different solvent conditions. At $\alpha_{12}^R = 300$ ($\chi_{12} = 15.3$), we observe an intermediate phase characterized by the coexistence of threads and bundle-like structures along the flow direction, as shown in Figure 10a. With increasing α_{12}^R , the threads are further brought to approach to each other, and the bundle-like structures can be obtained, as shown in Figure 10b. However, in these systems, the phase separation is not complete

because shear flow suppresses the phase separation of the threads into bundles. The bundle structures with some defects along the flow direction can be only obtained when the solvent condition becomes even worse (for example, $\alpha_{12}^R = 400$, as shown in Figure 10c). When further decreasing the solvent quality, the bundle will also break into short bundle-like structures (i.e., the broken bundles as defined in ref 23) because of the strong interfacial tension, as shown in Figure 10d.

Therefore, by properly selecting the shear rates and the solvent conditions, we can obtain the bundle-like structures along the flow direction. However, it is not easy to obtain the relatively well-defined bundle structures along the flow direction since shear flow suppresses the phase separation of the threads into bundles. In other words, shear flow actually favors the formation of long threads along the flow direction.

CONCLUSIONS

In conclusion, we present a mesoscale nonequilibrium simulation model which is suitable to study the hierarchical self-assembly of soft discoidal systems under shear flows. The effect of steady shear on the self-assembled structures of soft disklike particles is successfully investigated with the aid of this nonequilibrium model. The weak noncovalent attraction allows disklike particles to self-assemble into short threads. Shear flow induces an orientation of the short threads along the flow direction, leads to interthread connections, and results in a transition from short threads to long threads. Shear induced ordered structures can be obtained in systems that no ordered structures can be found without shear. However, further phase separation of the threads into the bundle structures is suppressed by shear flow. Therefore, by properly tuning shear rates and the solvent conditions, shear flow can induce the self-assembly of soft disklike particles into one-dimensional long threads and bundle-like structures with defects along the flow direction. The relatively well-defined bundle structures along the flow direction can be only obtained when the solvent condition becomes even worse. Our study not only supplies an insight into the shear-induced self-assembled structures of soft disklike particles, but also may provide a mesoscopic simulation strategy to study the hierarchical self-assembly of soft anisotropic systems in flow field and design novel nanostructures. It should be noted that hydrodynamic interactions are not included in our simulations, which were argued to play a crucial role in the structural formation during colloidal phase separation.^{66,67} Hydrodynamic interactions may have no noticeable effect on the thread structures which are mainly driven by weak attraction, but may strongly affect the formation of bundles. A full understanding of hydrodynamic effects during the phase separation of the threads into bundles is important and will be the focus of our consecutive study.

ASSOCIATED CONTENT

S Supporting Information. Typical packing structures for the larger systems and the self-assembled structures along the flow directions Y and Z axes. This material is available free of charge via the Internet at <http://pubs.acs.org>.

AUTHOR INFORMATION

Corresponding Author

*E-mail: zwli@ciac.jl.cn; luzhy@jlu.edu.cn. Phone: 0086 431 88498017. Fax: 0086 431 88498026.

■ ACKNOWLEDGMENT

This work is supported by the National Science Foundation of China (20774036, 20974040, and 50930001) and China Postdoctoral Science Foundation funded project (20100480069). Z.W.L. gratefully acknowledges the support of K. C. Wong Education Foundation.

■ REFERENCES

- (1) Jonkheijm, P.; van der Schoot, P.; Schenning, A. P. H. J.; Meijer, E. W. *Science* **2006**, *313*, 80.
- (2) Keizer, H. M.; Sijbesma, R. P. *Chem. Soc. Rev.* **2005**, *34*, 226.
- (3) Palmer, L. C.; Stupp, S. I. *Acc. Chem. Res.* **2008**, *41*, 1674.
- (4) Klein, M. L.; Shinoda, W. *Science* **2008**, *321*, 798.
- (5) Srinivas, G.; Discher, D. E.; Klein, M. L. *Nat. Mater.* **2004**, *3*, 638.
- (6) Cui, H.; Chen, Z.; Zhong, S.; Wooley, K. L.; Pochan, D. J. *Science* **2007**, *317*, 647.
- (7) Glotzer, S. C. *Science* **2004**, *306*, 419.
- (8) Service, R. F. *Science* **2005**, *309*, 95.
- (9) Glotzer, S. C.; Solomon, M. J. *Nat. Mater.* **2007**, *6*, 557.
- (10) Whitesides, G. M.; Boncheva, M. *Proc. Natl. Acad. Sci. U.S.A.* **2002**, *99*, 4769.
- (11) Zhang, Z.; Glotzer, S. C. *Nano Lett.* **2004**, *4*, 1407.
- (12) Sciotino, F.; Bianchi, E.; Douglas, J. F.; Tartaglia, P. *J. Chem. Phys.* **2007**, *126*, 194903.
- (13) Huisman, B. A. H.; Bolhuis, P. G.; Fasolino, A. *Phys. Rev. Lett.* **2008**, *100*, 188301.
- (14) Walther, A.; Müller, A. H. E. *Soft Matter* **2008**, *4*, 663.
- (15) Chen, Q.; Whitmer, J. K.; Jiang, S.; Bae, S. C.; Luijten, E.; Granick, S. *Science* **2011**, *331*, 199.
- (16) Clark, T. D.; Tien, J.; Duffy, D. C.; Paul, K. E.; Whitesides, G. M. *J. Am. Chem. Soc.* **2001**, *123*, 7677.
- (17) Chakrabarti, D.; Wales, D. J. *Phys. Rev. Lett.* **2008**, *100*, 127801.
- (18) Srinivas, G.; Pitera, J. W. *Nano Lett.* **2008**, *8*, 611.
- (19) Li, Z.; Kesselman, E.; Talmon, Y.; Hillmyer, M. A.; Lodge, T. P. *Science* **2004**, *306*, 98.
- (20) Yan, J.-J.; Tang, R.-P.; Zhang, B.; Zhu, X.-Q.; Xi, F.; Li, Z.-C.; Chen, E.-Q. *Macromolecules* **2009**, *42*, 8451.
- (21) Colafemmina, G.; Recchia, R.; Ferrante, A. S.; Amin, S.; Palazzo, G. *J. Phys. Chem. B* **2010**, *114*, 7250.
- (22) Li, Z.-W.; Chen, L.-J.; Zhao, Y.; Lu, Z.-Y. *J. Phys. Chem. B* **2008**, *112*, 13842.
- (23) Li, Z.-W.; Sun, Z.-Y.; Lu, Z.-Y. *J. Phys. Chem. B* **2010**, *114*, 2353.
- (24) McWhirter, J. L.; Noguchia, H.; Gompper, G. *Proc. Natl. Acad. Sci. U.S.A.* **2009**, *106*, 6039.
- (25) Ripoll, M.; Winkler, R. G.; Gompper, G. *Phys. Rev. Lett.* **2006**, *96*, 188302.
- (26) Grandjean, J.; Mourchid, A. *Langmuir* **2008**, *24*, 2318.
- (27) Schmidt, G.; Nakatani, A. I.; Butler, P. D.; Karim, A.; Han, C. C. *Macromolecules* **2000**, *33*, 7219.
- (28) Ripoll, M.; Holmqvist, P.; Winkler, R. G.; Gompper, G.; Dhont, J. K. G.; Lettinga, M. P. *Phys. Rev. Lett.* **2008**, *101*, 168302.
- (29) Liu, W.; Qian, H.-J.; Lu, Z.-Y.; Li, Z.-S.; Sun, C.-C. *Phys. Rev. E* **2006**, *74*, 021802.
- (30) You, L.-Y.; Chen, L.-J.; Qian, H.-J.; Lu, Z.-Y. *Macromolecules* **2007**, *40*, 5222.
- (31) You, L.-Y.; He, Y.-D.; Zhao, Y.; Lu, Z.-Y. *J. Chem. Phys.* **2008**, *129*, 204901.
- (32) Yu, H.; Jiang, W. *Macromolecules* **2009**, *42*, 3399.
- (33) Wang, Z.; Jiang, W. *Soft Matter* **2010**, *6*, 3743.
- (34) Zhong, C.; Liu, D. *Macromol. Theory Simul.* **2007**, *16*, 141.
- (35) Lonetti, B.; Kohlbrecher, J.; Willner, L.; Dhont, J. K. G.; Lettinga, M. P. *J. Phys.: Condens. Matter* **2008**, *20*, 404207.
- (36) Dubash, N.; Cardiel, J.; Cheung, P.; Shen, A. Q. *Soft Matter* **2011**, *7*, 876.
- (37) Takeda, M.; Kusano, T.; Matsunaga, T.; Endo, H.; Shibayama, M.; Shikata, T. *Langmuir* **2011**, *27*, 1731.
- (38) Vermant, J.; Solomon, M. J. *J. Phys.: Condens. Matter* **2005**, *17*, R187.
- (39) Löwen, H. *J. Phys.: Condens. Matter* **2008**, *20*, 404201.
- (40) Qazi, S. J. S.; Rennie, A. R.; Wright, J. P.; Cockcroft, J. K. *Langmuir* **2010**, *26*, 18701.
- (41) Pujolle-Robic, C.; Noirez, L. *Nature* **2001**, *409*, 167.
- (42) Lin-Gibson, S.; Schmidt, G.; Kim, H.; Han, C. C.; Hobbie, E. K. *J. Chem. Phys.* **2003**, *119*, 8080.
- (43) Sarman, S.; Laaksonen, A. *Chem. Phys. Lett.* **2009**, *479*, 47.
- (44) Park, J.; Butler, J. E. *Macromolecules* **2010**, *43*, 2535.
- (45) Pryamitsyn, V.; Ganesan, V. *Macromolecules* **2009**, *42*, 7184.
- (46) Raez, J.; Morales, J. G.; Fenniri, H. *J. Am. Chem. Soc.* **2004**, *126*, 16298.
- (47) Hobbie, E. K.; Fry, D. J. *Phys. Rev. Lett.* **2006**, *97*, 036101.
- (48) Qazi, S. J. S.; Rennie, A. R.; Tucker, I.; Penfold, J.; Grillo, I. *J. Phys. Chem. B* **2011**, *115*, 3271.
- (49) Fodi, B.; Hentschke, R. *J. Chem. Phys.* **2000**, *112*, 6917.
- (50) Groot, R. D.; Warren, P. B. *J. Chem. Phys.* **1997**, *107*, 4423.
- (51) Allen, M. P.; Tildesley, D. J. *Computer Simulation of Liquids*: Clarendon Press: Oxford, U.K., 1987.
- (52) Berendsen, H. J. C.; Postma, J. P. M.; van Gunsteren, W. F.; DiNola, A.; Haak, J. R. *J. Chem. Phys.* **1984**, *81*, 3684.
- (53) Lees, A. W.; Edwards, S. F. *J. Phys. C: Solid State Phys.* **1972**, *5*, 1921.
- (54) Yuan, X.-F.; Allen, M. P. *Physica A* **1997**, *240*, 145.
- (55) Schmid, F. *Lect. Notes Phys.* **2006**, *704*, 211.
- (56) Hijazi, A.; Zoaeter, M. *Eur. Polym. J.* **2002**, *38*, 2207.
- (57) Chen, L.-J.; Lu, Z.-Y.; Qian, H.-J.; Li, Z.-S.; Sun, C.-C. *J. Chem. Phys.* **2005**, *122*, 104907.
- (58) Warner, M.; Flory, P. J. *J. Chem. Phys.* **1980**, *73*, 6327.
- (59) Lekkerkerker, H. N. W.; Coulon, P.; Vanderhaegen, R.; Deblieck, R. *J. Chem. Phys.* **1984**, *80*, 3427.
- (60) Surve, M.; Pryamitsyn, V.; Ganesan, V. *Macromolecules* **2007**, *40*, 344.
- (61) Gabriel, A. T.; Meyer, T.; Germano, G. *J. Chem. Theory Comput.* **2008**, *4*, 468.
- (62) Grzybowski, B. A.; Stone, H. A.; Whitesides, G. M. *Nature* **2000**, *405*, 1033.
- (63) Zewdie, H. *J. Chem. Phys.* **1998**, *108*, 2117.
- (64) Zewdie, H. *Phys. Rev. E* **1998**, *57*, 1793.
- (65) He, L.; Pan, Z.; Zhang, L.; Liang, H. *Soft Matter* **2011**, *7*, 1147.
- (66) Tanaka, H.; Araki, T. *Phys. Rev. Lett.* **2000**, *85*, 1793.
- (67) Tanaka, H. *J. Phys.: Condens. Matter* **2005**, *17*, S2795.